TRANSITIONS IN A SOFT-WALLED CHANNEL.

V. Kumaran
Department of Chemical Engineering,
Indian Institute of Science,
Bangalore 560 012, India.
kumaran@chemeng.iisc.ernet.in

S. S. Srinivas,
Department of Chemical Engineering,
Indian Institute of Science,
Bangalore 560 012, India.
sagar@chemeng.iisc.ernet.in

ABSTRACT

In a soft-walled channel, there is a dynamical instability due to the coupling between the fluid flow and the wall dynamics which leads to a transion to turbulence. The transition Reynolds number is lower than Re=1000 for a rigid channel if the wall elasticity is sufficiently small. The transition Reynolds number depends on the parameter $\Sigma = (\rho G h^2/\eta^2)$, where ρ and η are the fluid density and viscosity, G is the shear modulus of the wall material and h is the channel height. The characteristics of the flow after transition are studied using Particle Image Velocimetry (PIV) in a rectangular channel with walls made of polyacrylamide gel, in which one wall is fixed to a rigid substrate and the other wall is unconstrained. The channels have width about 1.3 cm, height (smallest dimension) about 0.6 mm and the length of the channel is about 14 cm. The channels are fabricated with soft polyacrylamide gel with shear modulus about 0.75 kPa. There is a soft-wall transition at a Reynolds number below 1200, where the flow is symmetric about the centerline, and the wall fluctuations are primarily tangential to the surface, and the velocity statistics are independent of downstream distance. As the Reynolds number is increased, there is a second wall-flutter transition at the top unrestrained surface alone, where the profiles of the mean and root-mean-square velocities are larger near the top surface. Downstream traveling waves, which decrease in amplitude, are observed at the top surface with fluctuations both normal and tangential to the surface. The von Karman plots of the near-wall velocity profiles indicate that there is no discernible viscous sub-layer for (yv_*/ν) as low as 2, where y is the distance from the wall, v_* is the friction velocity and ν is the kinematic viscosity. There is clear evidence of a logarithmic layer for soft-wall turbulence, but the von Karman constants are very different from those for the flow in a hard-walled channel. However, there is no evidence of a logarithmic layer after the wall-flutter transition as the Reynolds number is further increased.

INTRODUCTION

Linear stability studies of the flow past model flexible surfaces, usually considered as spring-backed plates, have found different modes of instability. In the initial studies of Benjamin (1960, 1963); Landahl (1962), these were classified into three types — the class A modes which are the rigid-wall Tollmien-Schlichting instability modified by surface flexibility, the class B modes which have wave speed close to the surface waves on the medium, and the class C or traveling wave flutter which is similar to the Kelvin-Helmholtz instability. Subsequently, Carpenter & Garrad (1985) and Carpenter & Garrad (1986) modified the classification to include the class B and class C modes into a category called flow-induced surface instabilities, which are qualitatively different from the Tollmien-Schlichting modes. Class A modes are stabilised by surface damping, and class B modes could be destabilised by damping in the surface. Moreover, the coalescence of the Tollmien-Schlichting modes and the traveling wave flutter could result in a powerful static divergence instability which could destabilise the flow. Thus, the linear stability studies suggested that surface compliance stabilises some modes of instability but destabilises other modes, and so surface compliance is unlikely to result in transition delay.

There have been relatively few numerical studies on turbulence modification due to the dynamical interaction between the fluid turbulence and a flexible surface. The studies of Xu *et al.* (2003) and Rempfer *et al.* (2003) on a spring-backed wall model using Direct Numerical Simulations reported relatively modest turbulence modification due to the wall motion. There does not seem to be any work on the turbulence modification due to a soft wall modeled as a visco-elastic continuum.

The pioneering experiments of Hansen & Hunston (1974), Hansen & Hunston (1983) and Gad-el Hak *et al.* (1985) have reported the 'static divergence' instability, a hydro-elastic instability due to the coupling between the fluid flow and a compliant surface in different experimental geometries. Hansen & Hunston (1974) considered a rotating disk geometry, where a disk coated with a compliant surface was rotated in a tank, while Hansen & Hunston

(1983) examined the boundary-layer flow over a flat plate coated with a compliant material. In the case of Gad-el Hak *et al.* (1985), a flat plate partially coated with a compliant surface was towed in a tank of water. Many of the important observations in these experiments are similar, though there are some differences. All studies report the appearance of waves on the compliant surface, when the dimensionless parameter $V(\rho/G)^{1/2}$ exceeds a critical value, where V is the free stream velocity relative to the solid surface, G is the shear modulus of the compliant surface, ρ is the density, and $(G/\rho)^{1/2}$ is the propagation velocity of shear waves in the solid. Hansen & Hunston (1983) reported the onset of waves on the surface both for turbulent and laminar flows. Gad-el Hak *et al.* (1985) observed an instability only for turbulent boundary layer flows; the instability was not observed for laminar flows even when the free stream velocity was two times the shear wave velocity. The waves were nearly stationary in the reference frame of the solid, and the wave amplitude was found to be larger than the viscous sub-layer thickness at the surface. The surface waves thereby increased the drag force in a manner similar to static surface roughness elements. Gad-el Hak *et al.* (1985) also reported that the heights of the large eddies near the surface were significantly larger when there were static divergence waves on the compliant surface.

The earliest studies on the transition in internal flows bounded by soft walls was carried out by Lahav *et al.* (1973) and Krindel & Silberberg (1979), who reported a reduction in the transition Reynolds number in comparison to the value of 2100 for a rigid tube. They also found that the transition Reynolds number decreased as the wall elasticity modulus decreased, and the transition appeared to be continuous, in contrast to the discontinuous transition in the flow through rigid tubes. Following this, linear stability studies were carried out (Kumaran (2000, 2003, 2015); Shankar (2015)) on the flow through soft tubes and channels, where the soft wall was modeled as a viscoelastic solid, and continuity of velocity and stress were imposed at the fluid-solid interface. The linear stability studies found different modes of destabilisation in both the high and low Reynolds number limits. The transition Reynolds number depends on the ratio of elastic and viscous stresses, $\Sigma = (\rho G R^2/\eta^2)$, where, R is the tube diameter/channel height, G is the shear modulus of wall material, η and ρ are the fluid viscosity and density respectively. At low Reynolds number, even in the absence of inertia, there is an instability when the parameter $(V\eta/GR)$ exceeds a critical value (Kumaran *et al.* (1994); Kumaran (1995); Shankar & Kumar (2004); Gkanis & Kumar (2003, 2005); Chokshi & Kumaran (2008)). The mechanism is the transfer of energy from the mean flow to the fluctuations due to the shear work done at the fluid-solid interface, and the transition Reynolds number is proportional to the parameter Σ in this case. At high Reynolds number, two different modes of instability have been identified. In the case of the inviscid instability (Kumaran (1996); Shankar & Kumaran (1999, 2000); Gaurav & Shankar (2009, 2010)), qualitatively similar to that in a rigid channel, an internal critical layer of thickness $\mathrm{Re}^{-1/3}$ within the flow where viscous stresses are important. The transition Reynolds number is influenced by the wall elasticity, and it scales as $\Sigma^{1/2}$. There is another mode of destabilisation not present in the flow past rigid surfaces, called the wall mode instability, where the viscous forces are important in a wall layer of thickness $\mathrm{Re}^{-1/3}$ at the wall (Kumaran (1998); Shankar & Kumaran (2001, 2002); Chokshi & Kumaran (2009)). The mechanism of destabilisation is the transfer of energy from the mean flow to the fluctuations due to the shear work at the surface, and the transition Reynolds number scales as $\Sigma^{3/4}$.

Experiments on the flow of very viscous silicone oil over a polymer gel have verified the low Reynolds number instability (Kumaran & Muralikrishnan (2000); Muralikrishnan & Kumaran (2002); Eggert & Kumar (2004); Shrivastava *et al.* (2008)). The wall mode instability at high Reynolds number has also been verified in experiments (Verma & Kumaran (2012, 2013)). The transition Reynolds number in experiments is in agreement with theoretical predictions, if the wall deformation due to the applied pressure gradient, and the consequent change in the mean velocity, are incorporated in the analysis. The transition Reynolds number in a flexible tube of diameter about 1 mm is found to be as low as 500, and that in a channel of height about 100 μm is as low as 200. The flow after transition has also been studied (Srinivas & Kumaran (2015)), and results indicate several similarities and differences with the turbulent flow in a rigid channel. There is a transition from a parabolic profile to a profile that is flatter at the center and steeper at the walls at the transition Reynolds number, and a sharp increase in the magnitudes of the fluctuating velocities. The stream-wise root mean square velocity, in particular, exhibits the characteristic maximum near the wall. The important differences include the asymmetry in the fluctuating velocities, where the root mean square velocity at the soft surface is much larger than that near the hard surface, the apparent non-zero value of the Reynolds stress at the wall, and the detection of wall fluctuations at the transition Reynolds number. Though a viscous sub-layer was not detected in the experiments, possibly due to the lack of resolution, a logarithmic layer was observed. However, the extent of the logarithmic layer, when expressed in wall units, was much smaller than that in a rigid channel, and the von Karman constants were also very different. The turbulent velocity fluctuations at a Reynolds number in the range 250-400 in a soft-walled channel, when scaled by suitable powers of the mean velocity, are larger than those in a rigid channel in the Reynolds number range 5000-20000.

EXPERIMENTAL METHODS

A rectangular bore is fabricated in a block of polyacrylamide gel, using the procedures used for outlined in Verma & Kumaran (2012) for a soft tube; the only difference is that a rectangular template is used instead of a tubular glass template. The rectangular bore has a width of about 1.3 cm and length about 14 cm and height (smallest dimension) of about 0.6 mm. Polyacrylamide gel is used, instead of polydimethylsiloxane (PDMS) that has been used in earlier studies (Verma & Kumaran (2012)), because it has a much lower shear modulus, and the shear modulus can be decreased by reducing the concentration of cross-linker during fabrication. The gel block is fixed to a rigid substrate at the bottom, while the top surface is unrestrained. Gels with two different shear moduli were fabricated. The gel with shear modulus about 0.75 kPa was used for fabricating the 'soft' channels, where the effect of fluid-wall coupling on transition and turbulence was studied. In order to provide a reference for the experiments, a gel with shear modulus 15.9 kPa was also fabricated; the elasticity modulus of this gel was sufficiently high that the wall flexibility did not affect the flow dynamics up to a Reynolds number of about

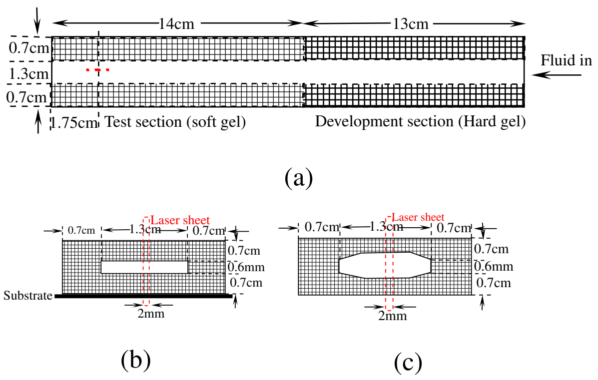

Figure 1. Schematic, not to scale, of the top view (a), cross section of the undeformed channel (b) and the deformed channel (c). In sub-figures (b) and (c), the laser sheet used for the PIV measurements is shown, and the images are taken from the side.

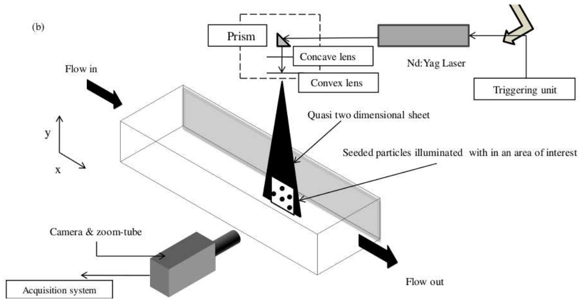

Figure 2. Configuration used for the velocity measurements.

900, which is the maximum Reynolds number that could be attained in the experiments.

A schematic of the tube configuration is shown in figure 1. The length of the test section, where the measurements are made, is about 14 cm. The walls of the channel in the soft section are made with shear modulus 0.75 kPa. Upstream of the test section, there is a development section of length about 13 cm where all four walls are made of hard gel with shear modulus about 15.9 kPa, so that there are no disturbances in the fluid when it enters the soft section. The flow is laminar in the hard section in all the experiments, and the flow conditioning in the hard section results in a fully developed parabolic profile at the entrance to the soft section. The configuration used for the experimental measurements is shown in figure 2. The PIV measurements are carried out using an IDT PIV system with an Nd-Yag laser (Solo-III, New Waver Research), laser sheet generating optics, and a SharpVisionTM 1500-EX CCD imager with a resolution of 1360×1036 pixels and a framing rate of 15 image pairs per second. The laser sheet is directed downwards along the central plane of the channel in the span-wise direction, as shown in figure 1 (b) and (c), and in figure 2. Glass beads of diameter 15-20 μm are used as seed particles. The measurements are carried out at a location close to the exit of the channel, as shown in figure 1 (a). The algorithms for determining the mean and root mean square velocities, and the validation, are provided in Srinivas & Kumaran (2015). Since the diameter of the glass beads is up to 20 μm, it is not possible to obtain results within a distance of about 20 μm from the walls of the channel. Therefore, we do not extrapolate the results for the fluctuating velocities to with 20 μm of the channel. Where the mean velocities are shown, they are extrapolated. In the co-ordinate system used, the flow is along the x direction, the vertical cross-stream dimension y is along the smallest channel dimension, and z is the span-wise direction along the width of the channel.

When there is flow through the channel, there is channel deformation and an expansion in height. While the expansion in height could be significant, from about 0.6 mm to about 0.8 mm, the slope of the wall is small, less than about 1% in all our experiments. Due to this, the laminar velocity profile does not differ from a parabolic profile by more than 2%. The Reynolds number is defined on the basis of the flow rate and the width of the channel,

$$\mathrm{Re} = \frac{\rho Q}{W \eta} \tag{1}$$

where ρ and η are the fluid density and viscosity, Q is the flow rate and W is the channel width, which is 1.3 cm from figure 1. This definition reduces to the usual definition of the Reynolds number, $\mathrm{Re} = (\rho \bar{v}_x h/\eta)$, where $\bar{v}_x$ is the average velocity and h is the channel height, for a rigid channel. However, equation 1 has the advantage that it is independent of channel height, and so it can be defined without ambiguity even when there is channel deformation.

RESULTS

The experimental measurements reveal that there are two different transitions in a soft-walled channel, both of which are at Reynolds number lower than the value of about 1000 for the transition in a hard-walled channel. These evolution of the mean velocity profile with an increase in the Reynolds number is shown in figure 3. The mean velocity profiles are in agreement with the parabolic velocity profile when the Reynolds number is less than about 300. When the Reynolds number exceeds 300, there is a distinct shift from a parabolic profile to a profile that is flatter at the center and steeper close to the walls. As the Reynolds number is increased, there is a second qualitative change in the form of the mean velocity profile. When the Reynolds number exceeds about 550, there is a distinct asymmetry in the mean velocity profile; the maximum of the velocity profile is closer to the top (unrestrained) wall in comparison to the bottom (fixed) wall. The two distinct transitions are also observed in the root mean square of the stream-wise fluctuating velocity v_x'. The level of fluctuations is low and featureless for Reynolds number less than about 300, but the profile of v_x' develops the characteristic near-wall maximum when the Reynolds number exceeds 300. As the Reynolds number is further increased, there is a distinct asymmetry when the Reynolds number exceeds 550, and the maximum near the top wall is significantly higher than that near the bottom wall.

Thus, the fluid velocity profiles indicate the presence of two distinct transitions, the soft-wall transition which is similar to that observed in Verma & Kumaran (2013) and Srinivas & Kumaran (2015), where there is a significant increase in the amplitude of the velocity fluctuations, but the profiles of the mean and the root mean square velocities are symmetric. There is no visible interface motion perpendicular to the surface, but motion tangential to the surface

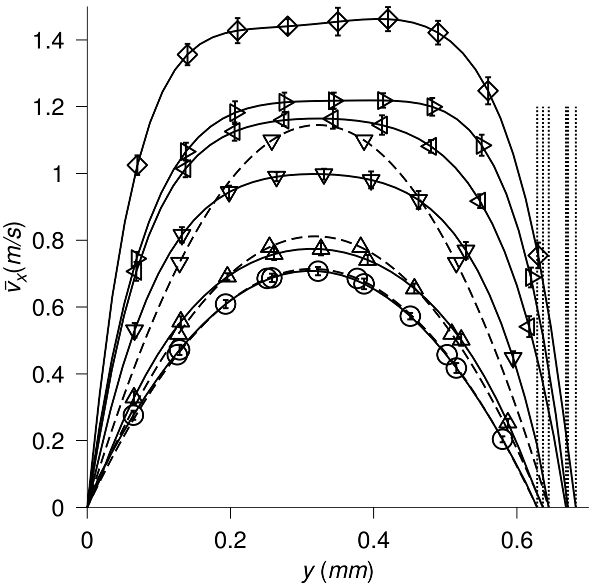

Figure 3. The mean velocity $\bar{v}_x$ as a function of the cross-stream distance y at Reynolds number 295 (○), 335 (△), 467 (∇), 546 (◁), 604 (▷), 734 (◇). The bottom wall is located at $y = 0$, and the location of the top wall at different Reynolds number is shown by the dashed lines at the right.

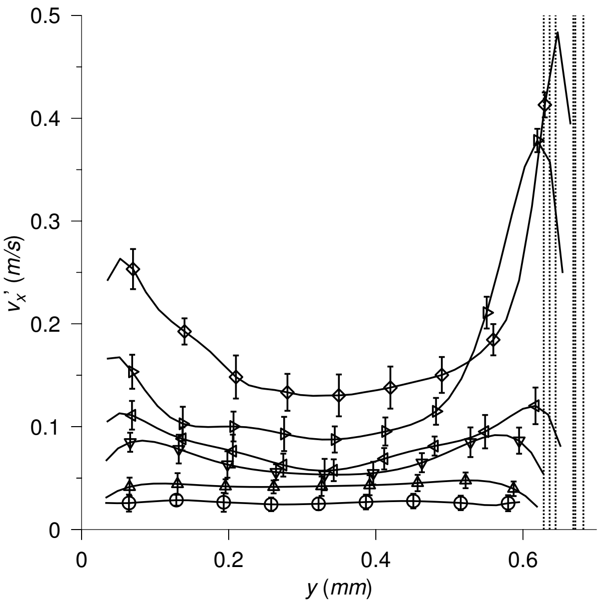

Figure 4. The root mean square of the stream-wise fluctuating velocity v_x' as a function of the cross-stream distance y at Reynolds number 295 (○), 335 (△), 467 (∇), 546 (◁), 604 (▷), 734 (◇). The bottom wall is located at $y = 0$, and the location of the top wall at different Reynolds number is shown by the dashed lines at the right. The dashed curves show the parabolic velocity profiles with the same average velocity as the experimental profile.

was detected, and as in the study of Srinivas & Kumaran (2015), there was a discontinuous increase in the amplitude of the fluctuations tangential to the surface at the transition Reynolds number. At the second 'wall flutter' transition, the velocity profiles are asymmetric, with the mean velocity larger near the top (unrestrained) boundary in comparison to the bottom (fixed) boundary. The velocity fluctuations are also found to be larger at the top boundary. In this case, there are visible downstream traveling waves at the top boundary observed in the experiments, and the amplitude of these waves decreases with downstream distance.

There are also some other unusual features in the profiles of the mean and root mean square velocities, 3 - 5. The mean velocity does extrapolate to zero according to the no-slip boundary condition at the two walls. However, the behaviour of the stream-wise root mean square velocity at the wall is not clear in figure 4. This velocity could be extrapolated to zero, while it could also be extrapolated to a non-zero value. Due to the lack of resolution in the near-wall region, it is not possible to determine the exact nature of the velocity fluctuations at the wall. However, the figure 5 seems to indicate that the Reynolds stress is non-zero at the wall — it is difficult to extrapolate the curves in figure 5 to zero Reynolds stress at the wall. Thus, it appears that the wall fluctuations do pay an important role in the generation of turbulent fluctuations. As shown in Srinivas & Kumaran (2015), the energy production rate has a maximum at the wall itself, rather than at a location close to the wall. Figure 5 suggests that the production of turbulent energy is due to the wall fluctuations, rather than the near-wall bursting of eddies.

The von-Karman plots of $(\bar{v}_x/v_*)$ vs. (yv_*/ν) are shown in figure 6. Here, the friction velocity $v_* = (\tau_w/\rho)^{1/2}$, where τ_w is the wall shear stress which includes the viscous stress and the Reynolds stress. Figure 6 shows that the mean velocity profile is linear close to the wall for a laminar flow at Re $= 295$. After the soft-wall transition, there is no discernible viscous sub-layer with a linear velocity variation for (yv_*/ν) as low as 2. However, in the range $3 < (yv_*/\nu) < 20$, there is a visible logarithmic layer after the soft-wall transition for Reynolds number greater than about 300. The von Karman constants are, however, very different from those for the flow in a rigid channel. As the Reynolds number is increased, we do not observe the logarithmic layer after the wall-flutter transition at a Reynolds number of about 550. Thus, a logarithmic layer is observed only when there is soft-wall transition; there is no logarithmic layer either at lower Reynolds number for a laminar flow, or at higher Reynolds number after the wall flutter transition.

Finally, we note that the wall flutter transition is observed only at the top unrestrained surface, and not at the bottom fixed surface. If the top surface is fixed to a rigid substrate, the soft-wall transition is still observed at the Reynolds number reported here, but the wall flutter transition is no longer observed. Thus, the wall flutter transition appears to be independent of the restraining conditions at the outer surface of the gel, but the soft-wall transition is independent of the outer restraining conditions.

CONCLUSIONS

Our experimental study has shown that there are two distinct transitions in the flow through a channel with soft walls, both at a Reynolds number lower than the hard-wall laminar-turbulent transition Reynolds number of about 1000.

1. The soft-wall transition, similar to the transition observed in microchannels at Reynolds number as low as 200 (Srinivas & Kumaran (2015); Kumaran & Bandaru

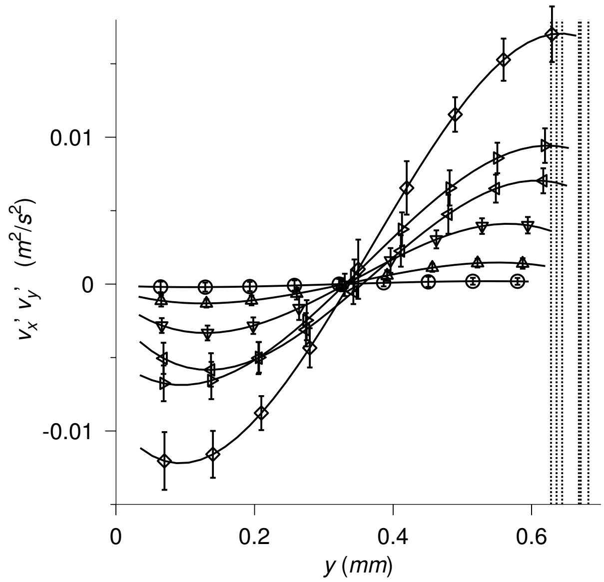

Figure 5. The Reynolds stressper unit mass $\langle v_x' v_y' \rangle$ as a function of the cross-stream distance y at Reynolds number 295 (○), 335 (△), 467 (∇), 546 (◁), 604 (▷), 734 (◇). The bottom wall is located at $y = 0$, and the location of the top wall at different Reynolds number is shown by the dashed lines at the right.

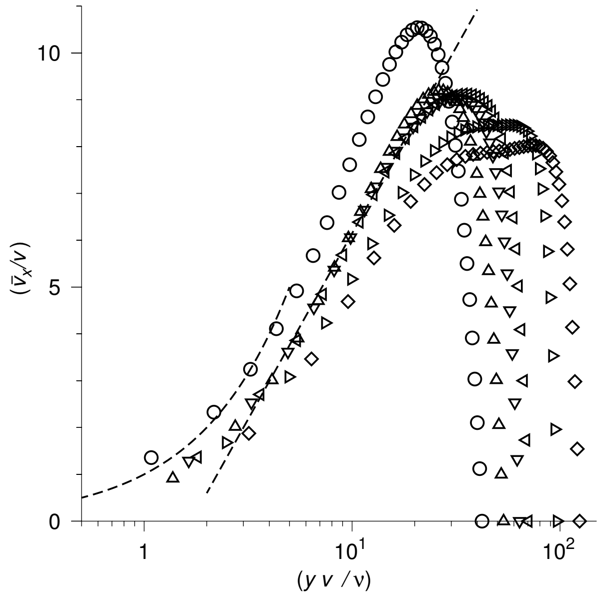

Figure 6. The von Karman plot of the scaled mean velocity $(\bar{v}_x/v_*)$ as a function of the scaled distance from the wall $(y v_*/\nu)$ at Reynolds number 295 (○), 335 (△), 467 (∇), 546 (◁), 604 (▷), 734 (◇). Here, y is the distance from the wall, $v_* = (\tau_w/\rho)^{1/2}$ is the friction velocity and ν is the kinematic viscosity. The dashed curve on the left is $(\bar{v}_x/v_*) = (y v_*/\nu)$, the dashed line on the right is $(\bar{v}_x/v_*) = 3.45 \log(y v_*/\nu) - 1.8$.

(2016)).

2. The wall-flutter transition, which shares many of the features of the hydroelastic instability (Hansen & Hunston (1974, 1983); Gad-el Hak *et al.* (1985)).

Both of these transitions have characteristics that are distinct from each other, and also distinct from those for the hard-wall transition.

Soft-wall transition

The most conspicuous feature after the soft-wall transition is the presence of discernible wall motion tangential to the surface in both the stream-wise and the span-wise directions, but no detectable wall motion perpendicular to the surface. This is accompanied by a rather large increase in the root mean square of the fluctuating velocities in both the stream-wise and wall-normal directions. As observed for the flow in a micro-channel in Srinivas & Kumaran (2015), the root mean square velocities appear to be non-zero at the wall when extrapolated. The Reynolds stress is certainly non-zero at the wall, indicating that the wall motion plays a significant role in generating fluid velocity fluctuations. The profiles of the velocity moments after the soft-wall transition are symmetric about the center line, indicating that the boundary conditions at the outer boundary of the soft wall are not relevant for the flow or wall dynamics — this implies that the displacement fluctuations penetrate only to a finite depth within the soft wall. (It should be noted that the wall thickness, about 7 mm, is much larger than the channel height). The flow characteristics are also independent of downstream location after a distance of about 5 cm from the start of the test section.

Wall-flutter transition

As the Reynolds number is increased, there is a wall flutter transition, in which there is a significant increase in the amplitude of the motion of the top (unrestrained) wall, and the displacement fluctuations parallel and perpendicular to the surface are comparable in magnitude. There is no normal motion detected, and there is no significant increase in the tangential wall fluctuations, at the bottom wall. The mean velocity is not symmetric about the center line of the channel, and the velocity maximum is closer to the top wall. The maximum in the stream-wise root mean square fluctuating velocity close to the top wall is significantly higher than that close to the bottom wall. The wall displacement and fluid velocity amplitudes also decrease with downstream distance, and the disturbances are in the form of traveling waves starting at the entrance to the soft section and decreasing in amplitude as they progress downstream. It is further found that the fluctuation amplitudes also do not increase monotonically with Reynolds number; the amplitude appears to first increase and then decrease indicating that this could be a resonance phenomenon.

The authors would like to thank the Department of Science and Technology, Government of India for financial support. This work forms a small portion of a more comprehensive study of the flow through soft channels with different dimensions and elasticity moduli which is under consideration in J. Fluid Mech.

REFERENCES

Benjamin, TB 1960 Effects of a flexible boundary on hydrodynamic stability. *J. Fluid Mech.* **9**, 513–532.

Benjamin, TB 1963 The three-fold classification of unstable disturbances in flexible surfaces bounding an inviscid flow. *J. Fluid Mech.* **16**, 436–450.

Carpenter, PW & Garrad, AD 1985 The hydrodynamic stability of the flow over kramer-type compliant surfaces.

part 1: Tollmien-schlichting instability. *J. Fluid Mech.* **155**, 465–510.

Carpenter, PW & Garrad, AD 1986 The hydrodynamic stability of the flow over kramer-type compliant surfaces. part 2: Flow induced surface instability. *J. Fluid Mech.* **170**, 199–232.

Chokshi, PP & Kumaran, V 2008 Weakly nonlinear analysis of viscous instability in flow past a neo-hookean surface. *Phys. Rev. E* **77**, 056303.

Chokshi, PP & Kumaran, V 2009 Weakly nonlinear stability analysis of a flow past a neo-hookean solid at arbitrary reynolds numbers. *Phys. Fluids* **21**, 014109.

Eggert, MD & Kumar, S 2004 Observations of instability, hysteresis and osciallations in low-reynolds-number flow past polymer gels. *J. Colloid Int. Sci* **274**, 238–242.

Gaurav & Shankar, V 2009 Stability of fluid flow through deformable neo-hookean tubes. *J. Fluid Mech.* **627**, 291–322.

Gaurav & Shankar, V 2010 Stability of pressure-driven flow in a deformable neo-hookean channel. *J. Fluid Mech.* **659**, 318–350.

Gkanis, V. & Kumar, S. 2003 Instability of creeping couette flow past a neo-hookean solid. *Phys. Fluids* **15**, 2864–2871.

Gkanis, V & Kumar, S 2005 Stability of pressure driven creeping flows in channels lined with a nonlinear elastic solid. *J. Fluid Mech.* **524**, 357–375.

Gad-el Hak, M, Blackwelder, RF & Riley, JJ 1985 On the interaction of compliant coatings with boundary layer flows. *J. Fluid Mech.* **140**, 257–280.

Hansen, RJ & Hunston, DL 1974 An experimental study of fluid turbulence over compliant surfaces. *J. Sound Vib.* **34**, 297–308.

Hansen, RJ & Hunston, DL 1983 Fluid-property effects on flow-generated waves on compliant surfaces. *J. Fluid Mech.* **133**, 161–177.

Krindel, P & Silberberg, A 1979 Flow through gel-walled tubes. *J. Colloid Int. Sci.* **71**, 39–50.

Kumaran, V 1995 Stability of the viscous flow of a fluid through a flexible tube. *J. Fluid Mech.* **294**, 259–281.

Kumaran, V 1996 Stability of an inviscid flow in a flexible tube. *J. Fluid Mech.* **320**, 1–17.

Kumaran, V 1998 Stability of wall modes in a flexible tube. *J. Fluid Mech.* **362**, 1–15.

Kumaran, V 2000 Classification of instabilities in the flow past flexible surfaces. *Curr. Sci.* **79**, 766–773.

Kumaran, V 2003 Hydrodynamic stability of flow through compliant channels and tubes. In *The Proceedings of IUTAM Symposium on Flow in Collapsible Tubes and Past Other Highly Compliant Boundaries* (ed. PW Carpenter & TJ Pedley). London: Kluwer Academic Publishers.

Kumaran, V 2015 Experimental studies on the flow through soft tubes and channels. *Sadhana* **40**, 911–923.

Kumaran, V. & Bandaru, P. 2016 Ultra-fast microfluidic mixing by soft-wall turbulence. *Chem. Eng. Sci.* **149**, 156–168.

Kumaran, V, Fredrickson, GH & Pincus, P 1994 Flow induced instability at the interface between a fluid and a gel at low reynolds number. *J. Phys. France II* **4**, 893–911.

Kumaran, V & Muralikrishnan, R 2000 Spontaneous growth of fluctuations in the viscous flow of a fluid past a soft interface. *Phys. Rev. Lett.* **84**, 3310–3313.

Lahav, J, Eliezer, N & Silberberg, A 1973 Gel-walled cylindrical channels as models for the microcirculation: dynamics of flow. *Biorheology* **10**, 595–604.

Landahl, MT 1962 On the stability of a laminar incompressible boundary layer over a flexible surface. *J. Fluid Mech.* **13**, 609–632.

Muralikrishnan, R & Kumaran, V 2002 Experimental study of the instability of the viscous flow past a flexible surface. *Phys. Fluids* **14**, 775–780.

Rempfer, D, Parsons, L, Xu, S & Lumley, J 2003 Theoretical approaches to the effect of wall compliance on turbulent flow. In *The Proceedings of IUTAM Symposium on Flow in Collapsible Tubes and Past Other Highly Compliant Boundaries* (ed. PW Carpenter & TJ Pedley). London: Kluwer Academic Publishers.

Shankar, V 2015 Stability of fluid flow through deformable tubes and channels: An overview. *Sadhana* **40**, 925–943.

Shankar, V & Kumar, S 2004 Instability of viscoelastic plane couette flow past a deformable wall. *J. Non-Newtonian Fluid Mech.* **116**, 371.

Shankar, V & Kumaran, V 1999 Stability of non-parabolic flows in a flexible tube. *J. Fluid Mech.* **395**, 211–236.

Shankar, V & Kumaran, V 2000 Stability of non-axisymmetric modes in a flexible tube. *J. Fluid Mech.* **407**, 291–314.

Shankar, V & Kumaran, V 2001 Asymptotic analysis of wall modes in a flexible tube revisited. *Euro. Phys. J. B* **19**, 607–622.

Shankar, V & Kumaran, V 2002 Stability of wall modes in the flow past a flexible surface. *Phys. Fluids* **14**, 2324–2338.

Shrivastava, A., Cussler, E. L. & Kumar, S. 2008 Mass transfer enhancement due to a soft elastic boundary. *Chem. Eng. Sci.* **63**, 4302–4305.

Srinivas, SS & Kumaran, V 2015 After transition in a soft-walled microchannel. *J Fluid Mech* **780**, 649–686.

Verma, MKS & Kumaran, V 2012 A dynamical instability due to fluid-wall coupling lowers the transition reynolds number in the flow through a flexible tube. *J. Fluid Mech.* **705**, 322–347.

Verma, MKS & Kumaran, V 2013 A multifold reduction in the transition reynolds number, and ultra-fast mixing, in a micro-channel due to a dynamical instability induced by a soft wall. *J. Fluid Mech.* **727**, 407–455.

Xu, S, Rempfer, D & Lumley, J 2003 Turbulence over a compliant surface: numerical simulation and analysis. *J. Fluid Mech.* **478**, 11–34.